Chemical Engineering Journal 490 (2024) 151698

Contents lists available at ScienceDirect

Chemical Engineering Journal

journal homepage: www.elsevier.com/locate/cej

Electrochemical carbon monoxide reduction at high current density: Cell configuration matters

Mohd Monis Ayyub, Attila Kormányos, Balázs Endrődi, Csaba Janáky *

Department of Physical Chemistry and Materials Science, University of Szeged, Rerrich Square 1, Szeged H-6720, Hungary

ARTICLE INFO

Keywords:
CO_2 reduction
Electrolyzers
Anion-exchange membranes
Copper

ABSTRACT

Electrochemical carbon monoxide reduction (COR) is an important link between the electrochemical CO_2-to-CO reduction technology and the renewable production of C_{2+} chemicals. Along with the development of catalyst materials for selective and efficient COR, it is imperative to optimize electrolysis conditions and cell parameters to efficiently reduce CO at industrially relevant current density and produce concentrated product streams. This study focuses on understanding fundamental differences in reaction selectivity during COR, when the same Cu catalyst was used in three different cell configurations, namely, microfluidic, hybrid anode zero-gap, and zero-gap electrolysers. In all cases, ethylene, acetate, ethanol, and propanol formation was confirmed at industrially relevant current densities (0.5–1.2 A cm^{-2}) at reasonable cell voltages, albeit with subtle differences. The local chemical environment at the electrode/electrolyte interface is very different in each configuration leading to different product distribution and product crossover to the anode. This stresses the importance of cell architecture and implies that comparing the catalytic activity of a catalyst studied with different cell configurations can lead to inconsistent conclusions.

1. Introduction

The dependency on fossil-fuel-derived energy of the Society has had drastic adverse effects on the Earth's environment, which make it critically important to develop alternative technologies that rely on cleaner and renewable energy sources. One such technology is the utilization of renewably produced electricity to convert atmospheric carbon dioxide (CO_2) to various fuels, chemicals, etc [1–3]. The field of electrochemical CO_2 reduction (CO2R) has taken large steps in the past decade with important discoveries of catalysts and electrochemical systems that perform at industrially relevant current densities to produce $2e^-$ reduction products (carbon monoxide and formate) [4–11]. The production of deeply reduced products (ethanol, acetate, propanol, etc.), however, is much more complex and lacks similar fundamental and technological advances. Copper is the only element that can catalyze the formation of C_{2+} chemicals at reasonable rates, however, it produces a complex mixture of hydrocarbons and oxygenates [12,13]. It is, therefore, crucial to selectively produce C_{2+} chemicals and even more important to understand the reaction mechanism to uncover intrinsic mechanistic details that can be used to design better catalysts and systems. A possible strategy for understanding the production of C_{2+} chemicals is studying electrochemical CO reduction (COR) since CO is a key intermediate in the production of hydrocarbons and oxygenates [14–17]. COR achieves higher C_{2+} Faradaic efficiency (FE) because the common C1 products (CH_4 and CH_3OH) are rarely formed due to favourable kinetics and surface coverages of *H and *CO intermediates [18–24].

A large fraction of research on CO2R/COR has been focused on exploring electrocatalyst materials and studying their catalytic activity using the H-cells [25–31]. This configuration, however, bears little similitude to the commercially important devices because of their static environment, in contrast to the dynamic nature of an electrolyser. Furthermore, the mass transport limits the current densities to < 10 mA cm^{-2} due to the very low solubility of CO at room temperature and in conventionally used electrolyte solutions and pressures [25,26]. Most recently, an increasing effort has been dedicated to studying COR in continuous flow cells that can overcome mass-transport limitations [29,32–34]. The important characteristic of flow cell electrolysers is the continuous feeding or circulation of gaseous reactant and liquid electrolyte that ensures an efficient supply of reactant CO, and efficient removal of reduced products away from the electrodes [16]. Another important aspect is the use of gas diffusion electrodes (GDE), which have porous hydrophobic channels that deliver reactant CO gas to the (partly)

* Corresponding author.
E-mail address: janaky@chem.u-szeged.hu (C. Janáky).

https://doi.org/10.1016/j.cej.2024.151698
Received 20 January 2024; Received in revised form 4 April 2024; Accepted 25 April 2024
Available online 26 April 2024

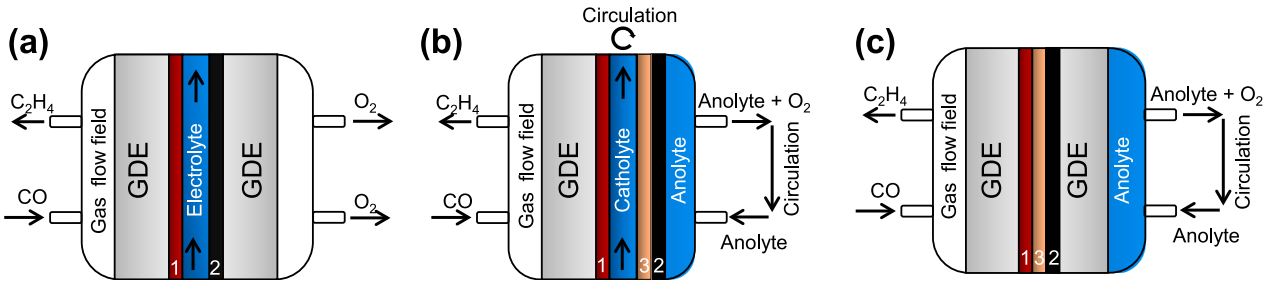

Fig. 1. Schematic representation of three different flow cell configurations (a) microfluidic, (b) hybrid anode zero-gap and (b) zero-gap. 1: cathode catalyst layer, 2: anode catalyst layer and 3: anion exchange membrane.

wetted catalyst particles and thereby efficiently reduces the diffusion length by several orders of magnitude [9]. Even though the importance of flow cell electrolysers has been clearly understood in CO2R, there is very little understanding of how different flow cell configurations affect the COR activity and selectivity [29,31,34]. The majority of the studies employ a flow cell configuration where the cathode GDE is in contact with a thin circulating catholyte layer that is separated from the anolyte layer by an ion exchange membrane [15,20,35]. Only a few studies report on the zero-gap cell configuration where the cathode (and the anode) is in direct contact with the membrane [36–40]. A recent study provided some initial insights into using electrochemical cell configurations with different ion transport configurations [36]. This study, however, was limited to a current density of 100 $mAcm^{-2}$, at high pressure (4 bar in zero-gap configuration) and did not provide a direct comparison of the different chemical environments in the different configurations.

The importance of the local chemical environment, in terms of reactant mass transport, the local concentration gradient of anionic or cationic species, and catalysts topology, in steering the selectivity of CO2R has been thoroughly reported in the literature [41–43]. To the best of our knowledge, there are, however, no studies focusing on the changes in the local chemical environment in different flow cell configurations for COR. The local chemical environment at the electrode/electrolyte interface will be very different in each configuration and, therefore, can affect the product formation, as presented below. In this study, three different cell configurations were studied under comparable conditions (in terms of cell temperature, electrolyte composition, and area-specific gas flow rate) with identical Cu nanoparticles as the cathode catalyst. The first two configurations (microfluidic and hybrid anode zero-gap), have a flowing catholyte in front of the cathode, while the third, zero-gap, configuration is operated without any catholyte. The presence/absence of a catholyte leads to substantial differences in product selectivity due to the changes in local cathode pH and local concentration of K^+ ions.

2. Methods and materials

2.1. Materials

All chemicals used in this study were purchased from Merck or VWR International. Chemicals of high purity (at least ACS reagent grade) were purchased and used without further purification. An aqueous dispersion of Capstone ST-110, was purchased from Chemours. Nafion dispersion (10 wt%) was purchased from Fuel Cell Store. Ultrapure water (18.2 MΩ cm) was used for the experiments, freshly produced using a Millipore Direct Q3 UV instrument. For COR measurements a 4.7 purity CO (Messer) cylinder was used..

2.2. Electrochemical experiments

Continuous-flow electrolysis experiments were performed in a two-electrode setup in three different cell configurations (Fig. 1).

Configuration I: Microfluidic cell, based on our previous work [44], which has a thin flowing electrolyte layer (flow rate = 1 cm^3 min^{-1}) between cathode and anode (single electrolyte solution, no membrane separation) (Fig. 1a and Fig. S1). CO gas is input from the back of the GDE through a 3 mm deep, 2 cm × 0.5 cm large cavities on the cathode plate serving as gas flow channels (flow rate = 23 sccm).

Configuration II: Hybrid anode zero-gap cell, where the anode is a catalyst-coated ion exchange membrane, while there is a thin layer of circulating electrolyte in front of the cathode catalyst layer, and the reactant CO gas is introduced from the back of cathode GDE (no gas flow pattern) (Fig. 1b and Fig. S1). It contained stainless steel (1.4571, 316-Ti) electrode current collectors, which have the CO gas inlet and outlet cutout but no flow field channel on the cathode plate and anolyte flow field channels on the anode plate. Threaded M5 inlet and outlet connection ports were formed on the cathode and anode for CO transport and anolyte flow, respectively. A poly (methyl methacrylate) (PMMA) separator (2 mm thickness) was used as the catholyte flow channel with a 3.5*3.5 cm cut out for the cathode GDE. The cathode GDE, and the PTFE gasket (d = 200 μm thickness) around it were placed between the cathode electrode and the PMMA separator. The anode CCM was mounted in the cell similarly. CO gas was fed to the cathode in a flow-by mode at a rate of u = 100 sccm through a ∅ = 6 mm polyurethane tube (Festo), while an electrolyte solution was directed between the two electrodes through a ∅= 4 mm polyurethane tube (Festo), at a flow rate of 4 cm^3 min^{-1}.

Configuration III: The third configuration is the membrane electrode assembly (MEA) configuration, also termed as zero-gap cell electrolyzer [4], which has a polymer electrolyte membrane sandwiched between the cathode and the anode (Fig. 1c and Fig. S1). The recirculated anolyte is continuously flowing in the anodic compartment (flow rate = 60 cm^3 min^{-1}) while the gaseous CO reactant (flow rate = 100 sccm) is being introduced from the back of the cathode via a gas flow pattern.

A Bronkhorst EL-FLOW Select F-201CV mass flow controller and a KF Technology NE-300 syringe pump were used for regulating the gas and the liquid flow rates, respectively.

The electrochemical measurements were controlled using a Biologic VMP300 type instrument. The COR products were analyzed using a Shimadzu Nexis GC-2030 gas-chromatograph (operated with 6.0 He carrier gas), equipped with a barrier discharge ionization (BID) detector and an automated 6-way valve injection system. The faradaic efficiency (FE) of the COR products was calculated from the GC results and the measured gas flow rate (Agilent ADM flow meter). Importantly, to avoid the pressure change in the gas line – which could lead to electrode flooding – a small vacuum pump was used to fill the sample loop of the injector, sampling the main gas stream. The liquid phase COR products in the anolyte and catholyte were quantified using a Bruker AV-III-500-HD NMR instrument. A calibration was performed for the studied compounds (ethanol, n-propanol and acetate) with the same background electrolyte concentration as in the real electrolysis samples. For the zero-gap configuration, the cathode gas flow field was washed with 5 mL water after electrolysis to collect liquid reduction products. In the

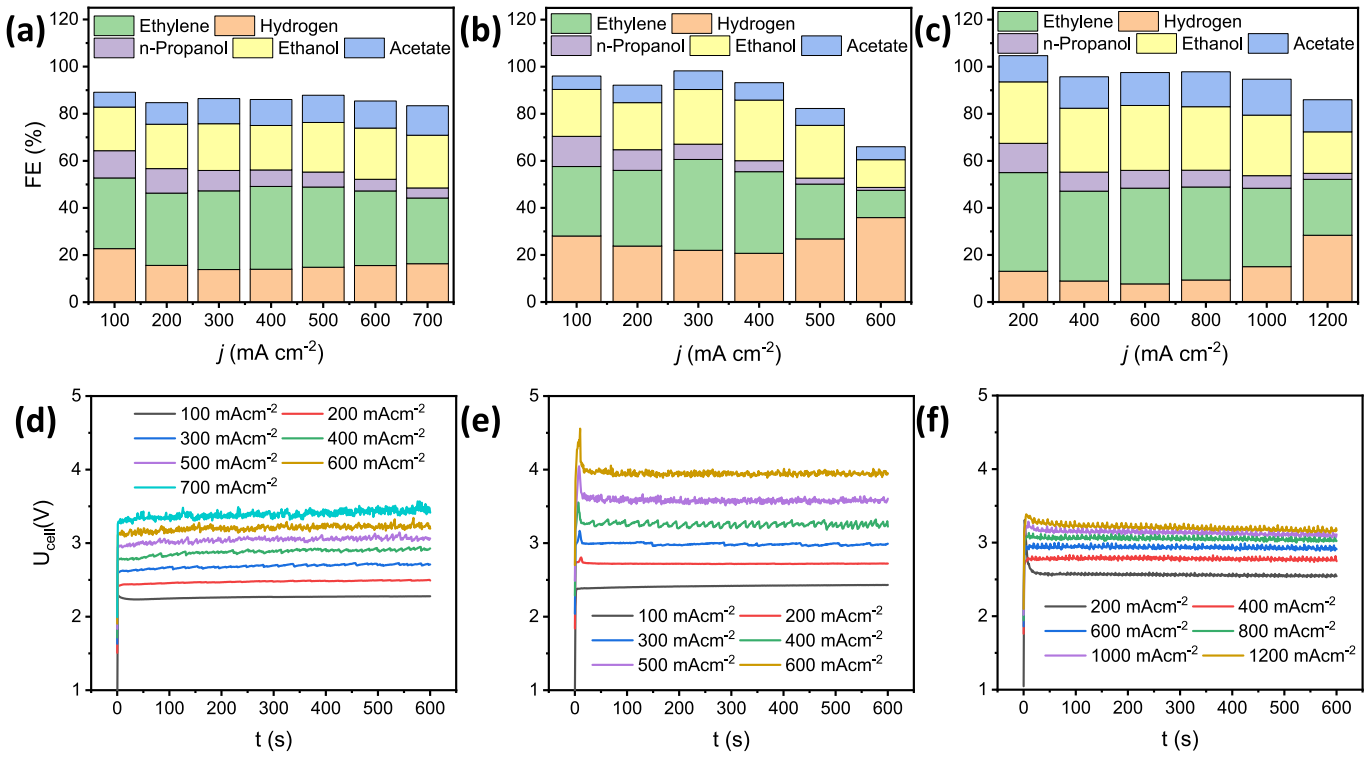

Fig. 2. Comparison of product distribution and cell voltages for CO electrolysis using 1 M KOH in (a and d) microfluidic, (b and e) hybrid anode zero-gap, and (c and f) zero-gap configurations, respectively. Electrolysis conditions: Cathode – Cu-5 % CST, Anode: Ir-15 % Nafion GDE (microfluidic), Ir-15 % PiperION CCM (hybrid), Ni foam (zero-gap), Membrane-PiperION.

case of the zero-gap configuration, at high current densities, the cell temperature gradually rises (up to ~ 35 °C during the 10 min measurements), however, that does not affect the product collection efficiency since the outlet gas stream goes through thermal water separator maintained at 2–4 °C that would condense any potentially evaporated liquid products. DMSO and phenol were used as internal standards [12].

2.3. Methods

Cathode GDE preparation: Copper nanopowder (25 nm, Merck) was dispersed in a 1:1 isopropanol water mixture with 5 wt% Capstone ST110 binder followed by sonication. This Cu dispersion was spray-coated using a hand-held airbrush on Sigracet 28BC gas diffusion layers (GDLs) preheated on a hotplate at 100 °C. The catalyst loading was maintained at 1 mg cm^{-2}.

Anode preparation:

For the microfluidic cell, the anode catalyst ink was prepared by dispersing IrO_x nanoparticle (Fuel-Cell Store) in a 1:1 isopropanol water mixture with 15 wt% Nafion binder. This IrO_x dispersion was spray-coated using a hand-held airbrush on Sigracet 28BC GDLs preheated on a hotplate at 100 °C. The catalyst loading was maintained at 1 mg cm^{-2}.

For the hybrid cell configuration, initially, Ir-15 wt% Nafion spray-coated on Ti frit was used as the anode, which was pressed against the PiperION anion-exchange membrane (AEM). During electrolysis, this led to the formation of bubbles and bulges in the AEM, causing the cell resistance to rise quickly. To avoid this, catalyst-coated membranes (CCM) were used as the anode. Catalyst ink was prepared by dispersing IrO_x nanoparticles (Fuel-Cell Store) in a 1:1 isopropanol water mixture with 15 wt% PiperION binder. This IrO_x dispersion was spray-coated using a hand-held airbrush on PiperION membrane (40 μm) preheated on a hotplate at 100 °C. The CCM was then activated by dipping in 1 M KOH for 24 h. The catalyst loading was maintained at 1 mg cm^{-2}.

Initially, for the zero-gap cell configuration, Ir-15 wt% Nafion coated on Ti frit was used as anode. As we experienced (in line with what was reported recently [45]), during electrolysis, the cathode quickly gets poisoned by the dissolution and subsequent deposition of Ir on the cathode, leading to a predominant hydrogen evolution reaction (Fig. S2). To avoid this, Ni foam (Recemat BV) was used as the anode, which was pre-treated by dipping in 5 M HCl for 30 min, followed by sonication in water to remove any NiO_x.

3. Results and discussion

3.1. Electrochemical CO reduction in different cell configurations

Alkaline COR involves the reduction of CO at the cathode, where H_2O acts as the proton source and electrons are injected through the external circuit, while hydroxide ions are oxidized to produce oxygen on the anode. The various reaction and product formation possibilities are tabulated in Table S1. In the microfluidic cell (Fig. 1a), the presence of a flowing electrolyte layer supports the quick removal of liquid products from the electrodes, ensuring that the COR products are not re-oxidized at the anode. Meanwhile, the flowing CO gas removes the gaseous products from the cathode. Chronovoltammetry experiments were performed at current densities (*j*) starting from 100 mA cm^{-2} (in 100 mA cm^{-2} increments) till cathode flooding was observed at 800 mA cm^{-2} (Table S2). Ethylene, n-propanol, ethanol, and acetate were the major COR products, while hydrogen formed as a by-product (Fig. 2a). An almost constant total COR selectivity of ~ 70 % was determined in the range of 200–700 mA cm^{-2}, with its peak value of ~ 73 % at 500 mA cm^{-2}. The cell voltages increase with increasing current densities (Fig. 2d).

In the hybrid anode zero-gap configuration (Fig. 1b), the presence of a membrane at first sight ensures that the liquid COR products do not come in contact with the anode, as the ion conduction in the system is - at this point - assumed to be maintained by transferring OH^- ions from the cathode to the anode. During chronovoltammetry measurements (at

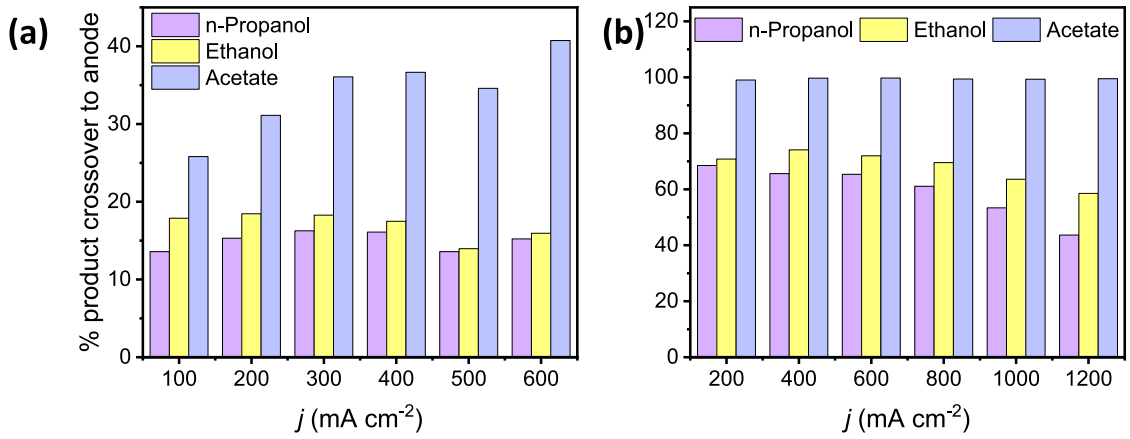

Fig. 3. Comparison of liquid product crossover in (a) hybrid anode zero-gap and (b) zero-gap cell configuration. Electrolysis conditions: Cathode – Cu-5 %CST, Anode: Ir-15 % PiperION CCM (hybrid) and Ni foam (zero-gap), Membrane-PiperION and Electrolyte- 1 M KOH.

current densities from 100 mA cm^{-2} till cathode flooding was observed at 600 mA cm^{-2}(Table S2)), ethylene, n-propanol, ethanol, and acetate were the major COR products (Fig. 2b) with a stable total FE_{COR} of ~ 70 % in the range of 100–400 mA cm^{-2} with its peak value of ~ 76 % at 300 mA cm^{-2}. The cell voltage increase in this case is also close to linear with the current density (Fig. 2e).

The zero-gap setup (Fig. 1c) ensured the lowest ohmic resistance among the studied cell architectures (Table S3) due to the intimate connection of the cell components. The water needed for the reduction reactions is supplied by the humidified CO, and the water transport from the anolyte through the AEM, while the excess OH^- produced at the cathode is transferred to the anode. Chronovoltammetry measurements were carried out at current densities starting from 200 mA cm^{-2} till cathode flooding was observed at 1200 mA cm^{-2} (Table S2)– a notably higher current density than in the other two cases, with the same major COR products (Fig. 2c). A stable total FE_{COR} of ~ 90 % in the range of 200–800 mA cm^{-2} and the highest FE_{COR} of 90 % at 600 mA cm^{-2} was measured.

In all three cases, an almost linear increase of the cell voltage with the current density was observed (Fig. 2d–f, Fig. S3). The lowest slope of 25 mV at every 100 mA cm^{-2} was determined for the zero-gap configuration, while it was 30 and 50 mV for the microfluidic and the hybrid anode zero-gap configurations, respectively. The overall FE of products for all three configurations is typically between 90–95 %. The missing 5–10 % FE could be due to liquid trapped in the GDE, oxidation of cathodic products at the anode, and undetected minor products. Because of the dynamic nature of the reactions, the loss of FE is more pronounced at high current densities where the cell is prone to flooding.

At the outset, the product palette is identical in all three reactor types, as was expected from using the exact same cathode catalyst. The stability of the cells, the maximum achievable current density, and the product selectivity, however, differ notably. Most importantly, the zero-gap cell configuration shows better stability and higher selectivity (~90 %) towards COR products compared to the other two configurations. In this case, the partial current densities for ethylene (320 mA cm^{-2}), ethanol (216 mA cm^{-2}), and acetate (120 mA cm^{-2}), are among the highest ones reported in the literature [15,18,35,36,46–53] despite the use of non-optimized, commercially available Cu catalyst. The zero-gap cell configurations also perform COR at industrially relevant current densities of up to 1.2 A cm^{-2} at a moderate cell voltage of ~ 3.2 V.

3.2. Liquid product crossover

The cathode and anode GDEs are separated in the microfluidic configuration by the 2 mm thick flowing electrolyte solution. Although there is a possibility of anodic oxidation of cathodically produced products, we did not observe any such phenomena because of the quick removal of liquid products by the presumably laminar flow of the electrolyte solution. On the long run, however, such single-pass, flow-through operation would consume a large amount of electrolyte solution and result in very dilute liquid product streams. Recirculating the electrolyte can improve the concentration of liquid products, but this will increase the possibility of anodic oxidation of COR products. A way to overcome this is to introduce a separator between the anode and the cathode. In the hybrid configuration, the anodic and cathodic compartments are separated by an AEM, which ensures the separation of reduction products from the anode and facilitates the movement of ions to maintain charge neutrality. The liquid products formed at the cathode get dissolved in the flowing catholyte, which is recirculated during electrolysis and thus can produce much more concentrated liquid product streams than the microfluidic configuration. Interestingly, it was observed that a considerable amount of liquid products were also transferred to the anodic compartment by crossing over through the AEM. Nearly 15–20 % of all the formed n-propanol and ethanol, while ~ 30 % acetate crosses over to the anode side, which shows that the PiperION AEM (not surprisingly) has a higher transfer rate for negatively charged acetate over neutral alcohols (Fig. 3a). An even higher amount of liquid product crossover was observed in the zero-gap configuration, where ~ 70 % of n-propanol and ethanol-, and 100 % of acetate crosses over (Fig. 3b). There is a possibility of anodic oxidation of ethanol to form acetate however, we did not observe any significant oxidation of ethanol in the present system (Table S4).

AEMs consist of hydrophilic cationic channels that assist the transport of anions. During COR, the major ion conduction through the AEM should be the transfer of the cathodically generated OH^- by a Grothus-type mechanism. However, based on our observations, the liquid products produced from COR also get transferred. The spatial separation of the membrane by a catholyte flow channel in the hybrid cell partly hinders this transport. In contrast, in the zero-gap cell, the majority of products cross over to the anode due to the close vicinity of the membrane to the cathode surface, where these species are formed, and, therefore, are present in high local concentrations. Recent reports show that the properties of the AEM can significantly affect the transport of alcohols and acetate through the membrane [46,54] The crossover of the negatively charged products is due to electromigration [55], while the neutral species crossover is because of diffusion owing to concentration gradient and electroosmotic drag. This transfer of COR products to the anode increases the separation cost of the products. This also points to the importance of analysing both the catholyte and anolyte streams to get a complete understanding of the catalyst's electrocatalytic property and the total mass balance of the process.

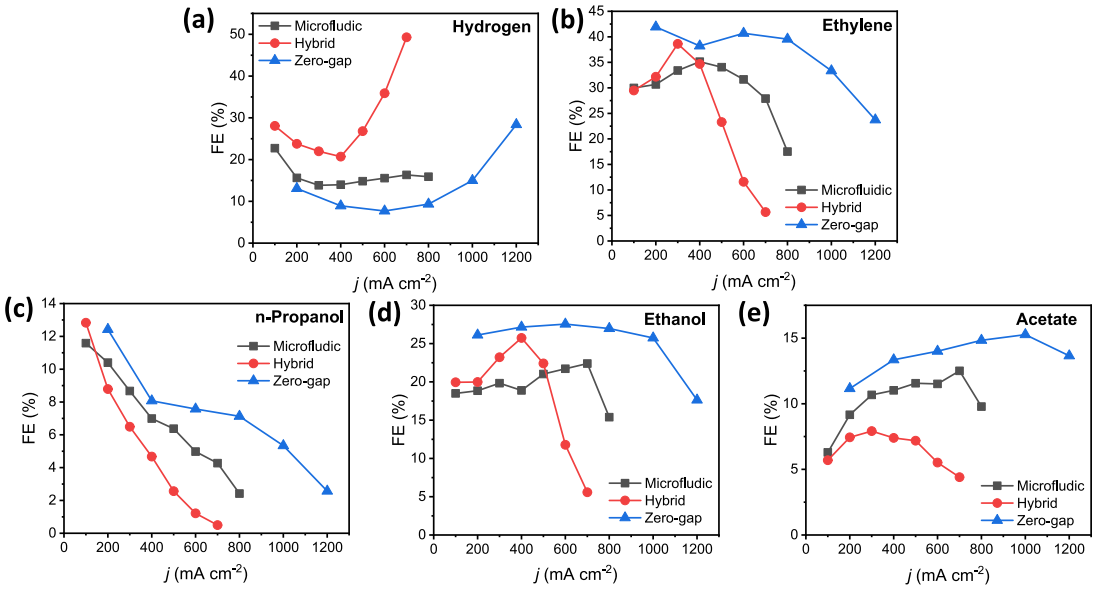

Fig. 4. Comparison of product distribution in different cell configurations at 1 M KOH concentration. Electrolysis conditions: Cathode – Cu-5 % CST, Anode: Ir-15 % Nafion GDE (microfluidic), Ir-15 % PiperION CCM (hybrid), Ni foam (zero-gap), Membrane-PiperION and Electrolyte- 1 M KOH.

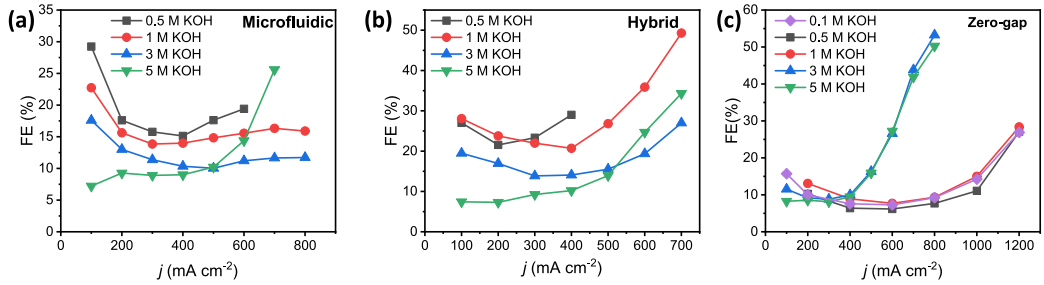

Fig. 5. Variation in FE_{H2} as a function of electrolyte concentration for (a) Microfluidic configuration, (b) hybrid anode zero-gap configuration, and (c) zero-gap configuration. Electrolysis conditions: Cathode – Cu-5% CST, Anode: Ir-15% Nafion GDE (microfluidic), Ir-15% PiperION CCM (hybrid), Ni foam (zero-gap), and Membrane-PiperION. Lines connecting the points have no causality and are only meant to serve as a guide to the eye.

3.3. Comparison of product distribution

Although qualitatively the same COR products formed in all cell configurations, a close analysis of product distribution as a function of current density shows subtle differences (Fig. 4). This stems from the difference in the local chemical environment at the electrode/electrolyte interface. Both configurations, which have a flowing catholyte in front of the cathode GDE (microfluidic and hybrid) exhibit higher hydrogen production rates compared to the zero-gap cell (and flooding occurs already at 600 mA cm^{-2}). At the same time, the zero-gap configuration exhibits higher stability, with signs of flooding only at very high current densities of 1200 mA cm^{-2}(Fig. 4a). As expected from the reduced HER rates, the highest overall COR product formation rate was observed in the zero-gap cell (Fig. 4b–e).

An important observation here is the pronounced acetate production in the zero-gap electrolyser compared to the other two configurations (Fig. 4e). Formerly, the formation of acetate has been directly correlated with the local cathode pH [49,56]. The selectivity-determining step towards acetate over other C_{2+} products is assumed to be the formation of a ketene intermediate, which gets desorbed from the catalyst surface. This ketene molecule can either react with OH^- from the electrolyte to form acetate or get re-adsorbed to the surface to form other C_{2+} products. This implies that the formation of acetate is directly related to the concentration of OH^- near the electrode surface. Zero-gap cell configuration has the highest production rates of acetate and, therefore, implies that the local cathode pH is higher in the zero-gap cell as compared to its counterparts with liquid catholytes. We briefly mention that most probably a pH gradient exists in the electrolyte bulk (electrolyte solution and/or membrane), and within the catalyst layer as well. As there is no clear measure (yet) of this gradient, we denote this as local pH.

3.4. Effect of electrolyte concentration

To further rationalize the distribution of products for each configuration, we studied COR using different KOH concentrations. Fig. 5 shows the variation of FE_{H2} at different electrolyte concentrations for all three configurations. For the microfluidic configuration, the increasing KOH concentration resulted in the gradual decrease of FE_{H2} (from ~ 30 % to ~ 7 % at 100 mA cm^{-2} when the KOH concentration changed from 0.5 to 5 M, Fig. 5a). A very similar trend was also observed for the hybrid cell (Fig. 5b). This is not surprising, as the cathode compartments of these cells are very similar, with only one important difference being the recirculation of the catholyte in the hybrid cell. This implies that the presence of COR products in the catholyte (at least in the studied timeframe) does not affect the COR process.

Interestingly, an almost completely reverse trend is observed for the zero-gap configuration: the FE_{H2} is very low even at low electrolyte (anolyte) concentration (Fig. 5c). At j = 600 mA cm^{-2}, FE_{H2} remains constant at ~ 7 % for 0.1, 0.5, and 1 M KOH, but for 3 and 5 M KOH it increases to ~ 27 %. At higher electrolyte concentrations, the cathode

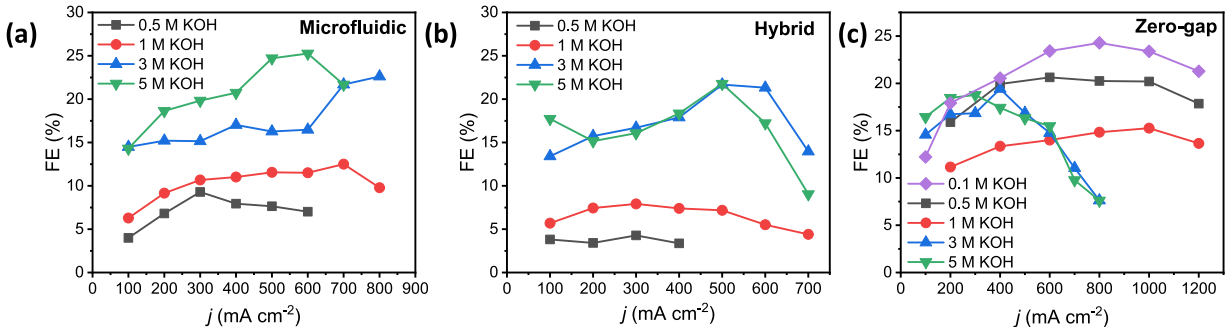

Fig. 6. Variation in acetate production as a function of electrolyte concentration for (a) Microfluidic configuration, (b) hybrid anode zero-gap configuration and (c) zero-gap configuration. Lines connecting the points have no causality and are only meant to serve as a guide to the eye.

floods already at 600 mA cm^{-2}, while for low KOH concentrations, cathode flooding is not observed till 1200 mA cm^{-2}. At low current density, no clear trend between the HER rates and the anolyte concentration can be observed. At high current density, rapid flooding was observed at high anolyte concentration, which could be due to a high flux and, subsequently, a high local concentration of K^+ ions in the cathode GDE structure. Galvanostatic electrochemical impedance spectroscopy (GEIS) measurements were carried out at 400 mA cm^{-2} for 0.5 – 5 M KOH and we observed that the double layer capacitance increases rapidly over 1 M KOH concentration, implying increased local concentration of K^+ at the cathode (Fig. S4). The presence of large amounts of weakly hydrated K^+ ions in the GDE can have a promoting or inhibiting effect on the HER rates depending on the pH and local K^+ concentration [57,58]. This could, therefore, be the reason behind increased HER rates and the concurrent flooding of the cathode at high anolyte concentrations.

A high local concentration of alkali metal cations at the cathode can stabilize reaction intermediates and modify the local electric field, thereby effectively promoting C_{2+} product formation in CO2R [42,59]. In the case of COR, however, Cu selectively produces only C_{2+} products. Therefore, a high local concentration of K^+ ions does not drastically change the product distribution. For the microfluidic and hybrid cell configurations, ethylene, n-propanol, and ethanol formation show no direct relation with KOH concentration (Figs. S5 and S6). However, acetate formation increases almost linearly with increasing electrolyte concentrations. For microfluidic configuration, $FE_{acetate}$ increases from ~ 7 % for 0.5 M KOH to ~ 25 % for 5 M KOH at 600 $mAcm^{-2}$ (Fig. 6a). Similarly, for the hybrid configuration, $FE_{acetate}$ increases from ~ 5 % for 0.5 M KOH to ~ 23 % for 5 M KOH (Fig. 6b).

Interestingly, the variation of product distribution with KOH concentration for the zero-gap configuration is different than the other two configurations (Fig. S7). The highest ethylene formation rate was observed for 0.1 M KOH, while the lowest for 5 M KOH. However, the FE of ethylene, ethanol, and n-propanol does not show any obvious direct correlation with anolyte concentration. The most striking difference was observed in the formation of acetate compared to other configurations (Fig. 6c). The highest acetate selectivity was observed for the lowest KOH concentration. The acetate production initially decreased with increasing KOH concentration to 1 M KOH, and then increased (Fig. S8). As expected from the proposed mechanism, acetate production selectivity should increase with the KOH concentration (electrolyte pH), and this is what is observed for the microfluidic and hybrid cell configurations. An opposite trend was observed in the zero-gap cell, which firstly indicates that the local cathode pH for the zero-gap cell remains largely unaffected by the anolyte pH and is only governed by the reduction reactions occurring at the cathode. Secondly, this implies that the local chemical environment is rather complicated in the zero-gap configuration and is governed by both the OH^- produced by COR and the species crossing over from the anode (H_2O and K^+). The changes in the acetate formation rate could therefore be due to a cumulative effect of high alkaline pH and an increased flux of K^+ ions.

An ideal AEM should be perm-selective to anions while being impermeable to cationic species. Actual AEMs, however, have been known to transfer cationic species (alkali cations) from the anolyte to the cathode surface, which are critically important for initiating and driving the selectivity of CO2R towards C_{2+} products [4,59,60]. The flux of K^+ through the membrane is dependent on the anolyte concentration as well as membrane transport properties [59,61]. According to the Donnan exclusion principle, if the anolyte concentration is comparable to the fixed charge density of the membrane, there is significant permeability of K^+ through the membrane, whereas a lower anolyte concentration leads to the strong exclusion of K^+ ions. The PiperION AEM used in this study has an ion-exchange capacity of 2.37 meq g^{-1} [62]. We expect that an anolyte concentration greater than or equal to this value would lead to increased cation crossover. In a recent paper, the charge concentration is estimated to be around 2 M, but the notable crossover of cations was already observed above 0.1 M concentration [59]. In this study, we use a similar but thicker membrane, that (together with the differences in the operating conditions) might explain the higher value in our case. Therefore, at low anolyte concentrations ($\leq$ 1 M KOH) the crossover of K^+ should be low and should increase for concentrations $>$ 1 M KOH. This could be linked to our observation on the variation of $FE_{acetate}$, as the concentration of the anolyte is increased to 1 M KOH, the crossover of H_2O increases while K^+ remains almost constant, leading to decreasing acetate production. For anolyte concentration $>$ 1 M KOH the flux of K^+ increases rapidly (as evidenced by rapid flooding at $j > 600$ $mAcm^{-2}$), and the acetate production increases again. These observations imply that acetate selectivity is not only dependent on the pH but also on the local K^+ ion concentration.

To test this hypothesis, COR was performed in the microfluidic configuration with an electrolyte containing 0.5 M K_2SO_4 in addition to 0.5 M KOH (Fig. S9). Increasing the K^+ concentration while keeping a constant pH does not affect the FE of hydrogen, n-propanol, and ethanol formation. However, a sharp decrease in $FE_{ethylene}$ and an increase in $FE_{acetate}$ were observed. The presence of K_2SO_4 in the electrolyte does not affect the HER rates implying that the local cathode pH does not change and therefore the changes in acetate selectivity are assumed to be primarily due to the increased K^+ concentration. This indicates that acetate selectivity depends on both the pH and K^+ concentration. This warrants further careful mechanistic investigations currently out of the scope of the present investigation.

4. Conclusion

This study sheds light on the effects of using different cell configurations for electrochemical COR. The microfluidic and hybrid anode zero-gap cells have a flowing catholyte layer and, hence, perform very similarly in terms of product distribution. Contrastingly, the product distribution and its variation with electrolyte concentration is very different for the zero-gap configuration. Solvation properties and

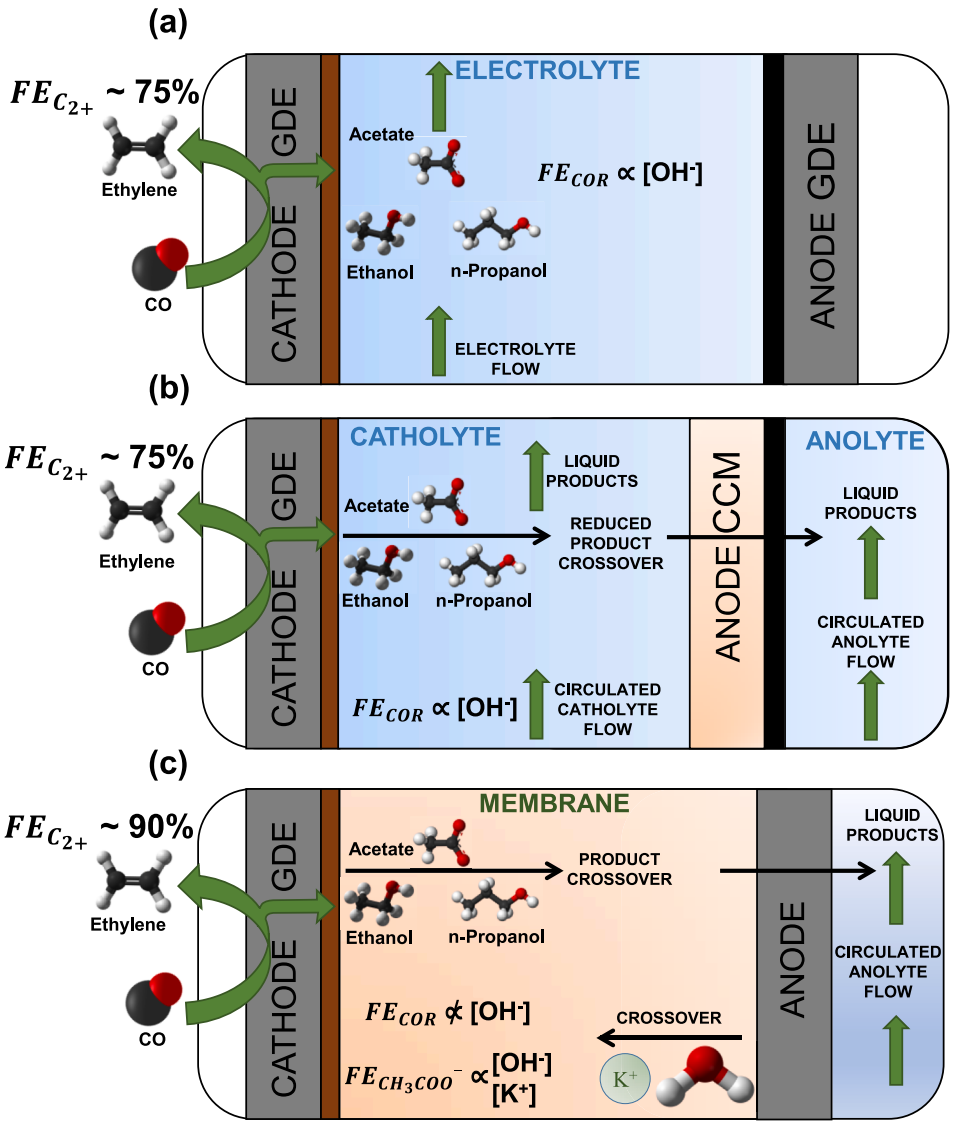

Fig. 7. Schematic illustration of various processes during COR in (a) microfluidic, (b) hybrid anode zero-gap, and (c) zero-gap configurations.

imperfections of the AEM (used to separate the cell compartments in the hybrid and the zero-gap cells) lead to the crossover of reduction products, water, and alkali cations through the membrane. Crossover of species is responsible for differences in the local chemical environment and, therefore, in product selectivity.

Differences in the local chemical environment of the cathode lead to differences in product selectivity, primarily hydrogen, and acetate. Local cathode pH in the microfluidic and hybrid cell configurations depends on the catholyte pH, while for the zero-gap cells, it depends mostly on the COR rate. Acetate selectivity is directly proportional to catholyte pH for the microfluidic and hybrid anode zero-gap configurations, while the relation is quite complex for the zero-gap cell. We hypothesize that the production of acetate, which has been otherwise only linked with cathode pH, is also directly dependent on the flux of K^+ through the membrane (Fig. 7).

Operating the cell at high current densities and at reasonable cell voltages depends on the fine balance of the anolyte concentration, which can reduce the cell voltage while also causing the rapid flooding of the cathode due to increased concentration of K^+. The careful tuning of these parameters could lead to the selective production of one COR product and a notably decreased rate of the competing hydrogen evolution reaction.

CRediT authorship contribution statement

Mohd Monis Ayyub: Writing – review & editing, Writing – original draft, Visualization, Methodology, Investigation, Formal analysis, Data curation. **Attila Kormányos:** Writing – review & editing, Visualization, Methodology, Investigation, Formal analysis. **Balázs Endrődi:** Writing – review & editing, Supervision, Project administration, Methodology, Formal analysis, Conceptualization. **Csaba Janáky:** Writing – review & editing, Supervision, Resources, Project administration, Methodology, Funding acquisition, Conceptualization.

Declaration of competing interest

The authors declare that they have no known competing financial interests or personal relationships that could have appeared to influence the work reported in this paper.

Data availability

Data will be made available on request.

Acknowledgements

Project no. RRF-2.3.1-21-2022-00009, titled National Laboratory for Renewable Energy has been implemented with the support provided by the Recovery and Resilience Facility of the European Union within the framework of Programme Széchenyi Plan Plus. This project has received funding under the European Union's Horizon 2020 research and innovation program from the FlowPhotoChem project (Grant Agreement No. 862453). A. K. acknowledges the financial support from the János Bolyai Research Scholarship of the Hungarian Academy of Sciences. The study was also supported by the ÚNKP-23-5-SZTE-671 New National Excellence Program of the Ministry for Culture and Innovation from the source of the National Research, Development and Innovation Fund." Authors acknowledge Egon Kecsenovity and Péter Tamás Turi for electrochemical cell designs.

Appendix A. Supplementary data

Supplementary data to this article can be found online at https://doi.org/10.1016/j.cej.2024.151698.

References

[1] P. De Luna, C. Hahn, D. Higgins, S.A. Jaffer, T.F. Jaramillo, E.H. Sargent, What would it take for renewably powered electrosynthesis to displace petrochemical processes? Science 364 (2019) https://doi.org/10.1126/science.aav3506.

[2] A. Raya-Imbernón, A.A. Samu, S. Barwe, G. Cusati, T. Fődi, B.M. Hepp, C. Janáky, Renewable Syngas Generation via Low-Temperature Electrolysis, Opportunities and Challenges, ACS Energy Lett. (2023) 288–297, https://doi.org/10.1021/acsenergylett.3c02446.

[3] H. Shin, K.U. Hansen, F. Jiao, Techno-economic assessment of low-temperature carbon dioxide electrolysis, Nat. Sustain. 4 (2021) 911–919, https://doi.org/10.1038/s41893-021-00739-x.

[4] B. Endrődi, A. Samu, E. Kecsenovity, T. Halmágyi, D. Sebők, C. Janáky, Operando cathode activation with alkali metal cations for high current density operation of water-fed zero-gap carbon dioxide electrolysers, Nat. Energy 6 (2021) 439–448, https://doi.org/10.1038/s41560-021-00813-w.

[5] B. Endrődi, E. Kecsenovity, A. Samu, F. Darvas, R.V. Jones, V. Török, A. Danyi, C. Janáky, Multilayer Electrolyzer Stack Converts Carbon Dioxide to Gas Products at High Pressure with High Efficiency, ACS Energy Lett. 4 (2019) 1770–1777, https://doi.org/10.1021/acsenergylett.9b01142.

[6] B. Endrődi, G. Bencsik, F. Darvas, R. Jones, K. Rajeshwar, C. Janáky, Continuous-flow electroreduction of carbon dioxide, Prog. Energy Combust. Sci. 62 (2017) 133–154, https://doi.org/10.1016/j.pecs.2017.05.005.

[7] G.L. De Gregorio, T. Burdyny, A. Loiudice, P. Iyengar, W.A. Smith, R. Buonsanti, Facet-Dependent Selectivity of Cu Catalysts in Electrochemical CO $_2$ Reduction at Commercially Viable Current Densities, ACS Catal. 10 (2020) 4854–4862, https://doi.org/10.1021/acscatal.0c00297.

[8] F.P. García de Arquer, C.-T. Dinh, A. Ozden, J. Wicks, C. McCallum, A.R. Kirmani, D.-H. Nam, C. Gabardo, A. Seifitokaldani, X. Wang, Y.C. Li, F. Li, J. Edwards, L. J. Richter, S.J. Thorpe, D. Sinton, E.H. Sargent, CO_2 electrolysis to multicarbon products at activities greater than 1 A cm−2, Science 367 (2020) 661–666, https://doi.org/10.1126/science.aay4217.

[9] T. Burdyny, W.A. Smith, CO_2 reduction on gas-diffusion electrodes and why catalytic performance must be assessed at commercially-relevant conditions, Energ. Environ. Sci. 12 (2019) 1442–1453, https://doi.org/10.1039/C8EE03134G.

[10] I.E.L. Stephens, K. Chan, A. Bagger, S.W. Boettcher, J. Bonin, E. Boutin, A. K. Buckley, R. Buonsanti, E.R. Cave, X. Chang, S.W. Chee, A.H.M. da Silva, P. de Luna, O. Einsle, B. Endrődi, M. Escudero-Escribano, J.V. Ferreira de Araujo, M. C. Figueiredo, C. Hahn, K.U. Hansen, S. Haussener, S. Hunegnaw, Z. Huo, Y. J. Hwang, C. Janáky, B.S. Jayathilake, F. Jiao, Z.P. Jovanov, P. Karimi, M.T. M. Koper, K.P. Kuhl, W.H. Lee, Z. Liang, X. Liu, S. Ma, M. Ma, H.-S. Oh, M. Robert, B.R. Cuenya, J. Rossmeisl, C. Roy, M.P. Ryan, E.H. Sargent, P. Sebastián-Pascual, B. Seger, L. Steier, P. Strasser, A.S. Varela, R.E. Vos, X. Wang, B. Xu, H. Yadegari, Y. Zhou, 2022 roadmap on low temperature electrochemical CO2 reduction, J. Phys. Energy 4 (2022) 042003, https://doi.org/10.1088/2515-7655/ac7823.

[11] Y. Lei, Z. Wang, A. Bao, X. Tang, X. Huang, H. Yi, S. Zhao, T. Sun, J. Wang, F. Gao, Recent advances on electrocatalytic CO_2 reduction to resources: Target products, reaction pathways and typical catalysts, Chem. Eng. J. 453 (2023) 139663, https://doi.org/10.1016/j.cej.2022.139663.

[12] K.P. Kuhl, E.R. Cave, D.N. Abram, T.F. Jaramillo, New insights into the electrochemical reduction of carbon dioxide on metallic copper surfaces, Energ. Environ. Sci. 5 (2012) 7050, https://doi.org/10.1039/c2ee21234j.

[13] L. Wang, D.C. Higgins, Y. Ji, C.G. Morales-Guio, K. Chan, C. Hahn, T.F. Jaramillo, Selective reduction of CO to acetaldehyde with CuAg electrocatalysts, PNAS 117 (2020) 12572–12575, https://doi.org/10.1073/pnas.1821683117.

[14] Y. Hori, A. Murata, R. Takahashi, S. Suzuki, Electroreduction of carbon monoxide to methane and ethylene at a copper electrode in aqueous solutions at ambient temperature and pressure, J. Am. Chem. Soc. 109 (1987) 5022–5023, https://doi.org/10.1021/ja00250a044.

[15] M. Jouny, W. Luc, F. Jiao, High-rate electroreduction of carbon monoxide to multi-carbon products, Nat. Catal. 1 (2018) 748–755, https://doi.org/10.1038/s41929-018-0133-2.

[16] M. Jouny, G.S. Hutchings, F. Jiao, Carbon monoxide electroreduction as an emerging platform for carbon utilization, Nat. Catal. 2 (2019) 1062–1070, https://doi.org/10.1038/s41929-019-0388-2.

[17] X. Wang, J.F. de Araújo, W. Ju, A. Bagger, H. Schmies, S. Kühl, J. Rossmeisl, P. Strasser, Mechanistic reaction pathways of enhanced ethylene yields during electroreduction of CO_2–CO co-feeds on Cu and Cu-tandem electrocatalysts, Nat. Nanotechnol. 14 (2019) 1063–1070, https://doi.org/10.1038/s41565-019-0551-6.

[18] T. Möller, M. Filippi, S. Brückner, W. Ju, P. Strasser, A CO2 electrolyzer tandem cell system for CO2-CO co-feed valorization in a Ni-N-C/Cu-catalyzed reaction cascade, Nat. Commun. 14 (2023) 5680, https://doi.org/10.1038/s41467-023-41278-7.

[19] A. Verdaguer-Casadevall, C.W. Li, T.P. Johansson, S.B. Scott, J.T. McKeown, M. Kumar, I.E.L. Stephens, M.W. Kanan, I. Chorkendorff, Probing the Active Surface Sites for CO Reduction on Oxide-Derived Copper Electrocatalysts, J. Am. Chem. Soc. 137 (2015) 9808–9811, https://doi.org/10.1021/jacs.5b06227.

[20] L. Wang, S.A. Nitopi, E. Bertheussen, M. Orazov, C.G. Morales-Guio, X. Liu, D. C. Higgins, K. Chan, J.K. Nørskov, C. Hahn, T.F. Jaramillo, Electrochemical Carbon Monoxide Reduction on Polycrystalline Copper: Effects of Potential, Pressure, and pH on Selectivity toward Multicarbon and Oxygenated Products, ACS Catal. 8 (2018) 7445–7454, https://doi.org/10.1021/acscatal.8b01200.

[21] T. Burdyny, S. Subramanian, J. Kok, P. Gholkar, A.S. Kumar, H.-P.-I. Van Montfort, R. Kortlever, A. Urakawa, B. Dam, CO residence time modulates multi-carbon formation rates in a zero-gap Cu based CO_2 electrolyzer, Res, Sq, 2024.

[22] R. Xia, J.-J. Lv, X. Ma, F. Jiao, Enhanced multi-carbon selectivity via CO electroreduction approach, J. Catal. 398 (2021) 185–191, https://doi.org/10.1016/j.jcat.2021.03.034.

[23] N.S. Romero Cuellar, K. Wiesner-Fleischer, M. Fleischer, A. Rucki, O. Hinrichsen, Advantages of CO over CO2 as reactant for electrochemical reduction to ethylene, ethanol and n-propanol on gas diffusion electrodes at high current densities, Electrochim. Acta 307 (2019) 164–175, https://doi.org/10.1016/j.electacta.2019.03.142.

[24] C.-T. Dinh, T. Burdyny, M.G. Kibria, A. Seifitokaldani, C.M. Gabardo, F.P. García de Arquer, A. Kiani, J.P. Edwards, P. De Luna, O.S. Bushuyev, C. Zou, R. Quintero-Bermudez, Y. Pang, D. Sinton, E.H. Sargent, CO $_2$ electroreduction to ethylene via hydroxide-mediated copper catalysis at an abrupt interface, Science 360 (2018) 783–787, https://doi.org/10.1126/science.aas9100.

[25] L. Wang, S. Nitopi, A.B. Wong, J.L. Snider, A.C. Nielander, C.G. Morales-Guio, M. Orazov, D.C. Higgins, C. Hahn, T.F. Jaramillo, Electrochemically converting carbon monoxide to liquid fuels by directing selectivity with electrode surface area, Nat. Catal. 2 (2019) 702–708, https://doi.org/10.1038/s41929-019-0301-z.

[26] C.W. Li, J. Ciston, M.W. Kanan, Electroreduction of carbon monoxide to liquid fuel on oxide-derived nanocrystalline copper, Nature 508 (2014) 504–507, https://doi.org/10.1038/nature13249.

[27] H. Bao, Y. Qiu, X. Peng, J. Wang, Y. Mi, S. Zhao, X. Liu, Y. Liu, R. Cao, L. Zhuo, J. Ren, J. Sun, J. Luo, X. Sun, Isolated copper single sites for high-performance electroreduction of carbon monoxide to multicarbon products, Nat. Commun. 12 (2021) 238, https://doi.org/10.1038/s41467-020-20336-4.

[28] J. Li, K. Chang, H. Zhang, M. He, W.A. Goddard, J.G. Chen, M.-J. Cheng, Q. Lu, Effectively Increased Efficiency for Electroreduction of Carbon Monoxide Using Supported Polycrystalline Copper Powder Electrocatalysts, ACS Catal. 9 (2019) 4709–4718, https://doi.org/10.1021/acscatal.9b00099.

[29] D. Wu, F. Jiao, Q. Lu, Progress and Understanding of CO $_2$ /CO Electroreduction in Flow Electrolyzers, ACS Catal. 12 (2022) 12993–13020, https://doi.org/10.1021/acscatal.2c03348.

[30] J. Choi, M.J. Kim, S.H. Ahn, I. Choi, J.H. Jang, Y.S. Ham, J.J. Kim, S.-K. Kim, Electrochemical CO 2 reduction to CO on dendritic Ag–Cu electrocatalysts prepared by electrodeposition, Chem. Eng. J. 299 (2016) 37–44, https://doi.org/10.1016/j.cej.2016.04.037.

[31] J.-B. Vennekoetter, R. Sengpiel, M. Wessling, Beyond the catalyst: How electrode and reactor design determine the product spectrum during electrochemical CO2 reduction, Chem. Eng. J. 364 (2019) 89–101, https://doi.org/10.1016/j.cej.2019.01.045.

[32] S. Overa, B.H. Ko, Y. Zhao, F. Jiao, Electrochemical Approaches for CO $_2$ Conversion to Chemicals: A Journey toward Practical Applications, Acc. Chem. Res. 55 (2022) 638–648, https://doi.org/10.1021/acs.accounts.1c00674.

[33] D.T. Whipple, E.C. Finke, P.J.A. Kenis, Microfluidic Reactor for the Electrochemical Reduction of Carbon Dioxide: The Effect of pH, Electrochem. Solid St. 13 (2010) B109, https://doi.org/10.1149/1.3456590.

[34] J. Park, Y. Ko, C. Lim, H. Kim, B.K. Min, K.-Y. Lee, J.H. Koh, H.-S. Oh, W.H. Lee, Strategies for CO_2 electroreduction in cation exchange membrane electrode assembly, Chem. Eng. J. 453 (2023) 139826, https://doi.org/10.1016/j.cej.2022.139826.

[35] J. Li, Z. Wang, C. McCallum, Y. Xu, F. Li, Y. Wang, C.M. Gabardo, C.-T. Dinh, T.-T. Zhuang, L. Wang, J.Y. Howe, Y. Ren, E.H. Sargent, D. Sinton, Constraining CO coverage on copper promotes high-efficiency ethylene electroproduction, Nat. Catal. 2 (2019) 1124–1131, https://doi.org/10.1038/s41929-019-0380-x.

[36] D.S. Ripatti, T.R. Veltman, M.W. Kanan, Carbon Monoxide Gas Diffusion Electrolysis that Produces Concentrated C2 Products with High Single-Pass Conversion, Joule 3 (2019) 240–256, https://doi.org/10.1016/j.joule.2018.10.007.

[37] J.A. Rabinowitz, D.S. Ripatti, R.G. Mariano, M.W. Kanan, Improving the Energy Efficiency of CO Electrolysis by Controlling Cu Domain Size in Gas Diffusion Electrodes, ACS Energy Lett. 7 (2022) 4098–4105, https://doi.org/10.1021/acsenergylett.2c01978.
[38] Y. Zhou, R. Ganganahalli, S. Verma, H.R. Tan, B.S. Yeo, Production of C_3–C_6 Acetate Esters via CO Electroreduction in a Membrane Electrode Assembly Cell, Angew. Chem. Int. Ed. 61 (2022), https://doi.org/10.1002/anie.202202859.
[39] S.H. Lee, I. Sullivan, D.M. Larson, G. Liu, F.M. Toma, C. Xiang, W.S. Drisdell, Correlating Oxidation State and Surface Area to Activity from *Operando* Studies of Copper CO Electroreduction Catalysts in a Gas-Fed Device, ACS Catal. 10 (2020) 8000–8011, https://doi.org/10.1021/acscatal.0c01670.
[40] X. Wang, P. Ou, A. Ozden, S.-F. Hung, J. Tam, C.M. Gabardo, J.Y. Howe, J. Sisler, K. Bertens, F.P. García de Arquer, R.K. Miao, C.P. O'Brien, Z. Wang, J. Abed, A. S. Rasouli, M. Sun, A.H. Ip, D. Sinton, E.H. Sargent, Efficient electrosynthesis of n-propanol from carbon monoxide using a Ag–Ru–Cu catalyst, Nat. Energy 7 (2022) 170–176, https://doi.org/10.1038/s41560-021-00967-7.
[41] K. Ye, G. Zhang, X.-Y. Ma, C. Deng, X. Huang, C. Yuan, G. Meng, W.-B. Cai, K. Jiang, Resolving local reaction environment toward an optimized CO_2-to-CO conversion performance, Energ. Environ. Sci. 15 (2022) 749–759, https://doi.org/10.1039/D1EE02966E.
[42] K. Ye, G. Zhang, B. Ni, L. Guo, C. Deng, X. Zhuang, C. Zhao, W.-B. Cai, K. Jiang, Steering CO2 electrolysis selectivity by modulating the local reaction environment: An online DEMS approach for Cu electrodes, Escience 3 (2023) 100143, https://doi.org/10.1016/j.esci.2023.100143.
[43] G. Zhang, K. Ye, B. Ni, K. Jiang, Steering the products distribution of CO2 electrolysis: A perspective on extrinsic tuning knobs, Chem. Catalysis 3 (2023) 100746, https://doi.org/10.1016/j.checat.2023.100746.
[44] A. Kormányos, B. Endrődi, Z. Zhang, A. Samu, L. Mérai, G.F. Samu, L. Janovák, C. Janáky, Local hydrophobicity allows high-performance electrochemical carbon monoxide reduction to C2+ products, EES Catalysis 1 (2023) 263–273, https://doi.org/10.1039/D3EY00006K.
[45] Q. Xu, S. Garg, A.B. Moss, M. Mirolo, I. Chorkendorff, J. Drnec, B. Seger, Identifying and alleviating the durability challenges in membrane-electrode-assembly devices for high-rate CO electrolysis, Nat. Catal. 6 (2023) 1042–1051, https://doi.org/10.1038/s41929-023-01034-y.
[46] S. Overa, B.S. Crandall, B. Shrimant, D. Tian, B.H. Ko, H. Shin, C. Bae, F. Jiao, Enhancing acetate selectivity by coupling anodic oxidation to carbon monoxide electroreduction, Nat. Catal. 5 (2022) 738–745, https://doi.org/10.1038/s41929-022-00828-w.
[47] S. Guo, Y. Liu, Y. Huang, H. Wang, E. Murphy, L. Delafontaine, J. "Loki" Chen, I. V. Zenyuk, P. Atanassov, Promoting Electrolysis of Carbon Monoxide toward Acetate and 1-Propanol in Flow Electrolyzer, ACS Energy Lett. 8 (2023) 935–942. https://doi.org/10.1021/acsenergylett.2c02502.
[48] P. Zhu, C. Xia, C.-Y. Liu, K. Jiang, G. Gao, X. Zhang, Y. Xia, Y. Lei, H.N. Alshareef, T.P. Senftle, H. Wang, Direct and continuous generation of pure acetic acid solutions via electrocatalytic carbon monoxide reduction, PNAS 118 (2021), https://doi.org/10.1073/pnas.2010868118.
[49] W. Luc, X. Fu, J. Shi, J.-J. Lv, M. Jouny, B.H. Ko, Y. Xu, Q. Tu, X. Hu, J. Wu, Q. Yue, Y. Liu, F. Jiao, Y. Kang, Two-dimensional copper nanosheets for electrochemical reduction of carbon monoxide to acetate, Nat. Catal. 2 (2019) 423–430, https://doi.org/10.1038/s41929-019-0269-8.
[50] J. Li, A. Xu, F. Li, Z. Wang, C. Zou, C.M. Gabardo, Y. Wang, A. Ozden, Y. Xu, D.-H. Nam, Y. Lum, J. Wicks, B. Chen, Z. Wang, J. Chen, Y. Wen, T. Zhuang, M. Luo, X. Du, T.-K. Sham, B. Zhang, E.H. Sargent, D. Sinton, Enhanced multi-carbon alcohol electroproduction from CO via modulated hydrogen adsorption, Nat. Commun. 11 (2020) 3685, https://doi.org/10.1038/s41467-020-17499-5.
[51] M.P. Schellekens, S.J. Raaijman, M.T.M. Koper, P.J. Corbett, Temperature-dependent selectivity for CO electroreduction on copper-based gas-diffusion electrodes at high current densities, Chem. Eng. J. 483 (2024) 149105, https://doi.org/10.1016/j.cej.2024.149105.
[52] J. Chen, L. Chen, J. Chen, D. Wang, Y. Zhao, L. Wen, S. Xi, L. Wang, Enhancing CO diffusion for selective acetate production via CO reduction on copper catalyst, Appl Catal B 343 (2024) 123551, https://doi.org/10.1016/j.apcatb.2023.123551.
[53] K. Yao, J. Li, A. Ozden, H. Wang, N. Sun, P. Liu, W. Zhong, W. Zhou, J. Zhou, X. Wang, H. Liu, Y. Liu, S. Chen, Y. Hu, Z. Wang, D. Sinton, H. Liang, In situ copper faceting enables efficient CO2/CO electrolysis, Nat. Commun. 15 (2024) 1749, https://doi.org/10.1038/s41467-024-45538-y.
[54] B. Hasa, L. Cherniack, R. Xia, D. Tian, B.H. Ko, S. Overa, P. Dimitrakellis, C. Bae, F. Jiao, Benchmarking anion-exchange membranes for electrocatalytic carbon monoxide reduction, Chem. Catalysis 3 (2023) 100450, https://doi.org/10.1016/j.checat.2022.10.026.
[55] J. Zhang, W. Luo, A. Züttel, Crossover of liquid products from electrochemical CO2 reduction through gas diffusion electrode and anion exchange membrane, J. Catal. 385 (2020) 140–145, https://doi.org/10.1016/j.jcat.2020.03.013.
[56] H.H. Heenen, H. Shin, G. Kastlunger, S. Overa, J.A. Gauthier, F. Jiao, K. Chan, The mechanism for acetate formation in electrochemical CO (2) reduction on Cu: selectivity with potential, pH, and nanostructuring, Energ. Environ. Sci. 15 (2022) 3978–3990, https://doi.org/10.1039/D2EE01485H.
[57] A. Goyal, M.T.M. Koper, The Interrelated Effect of Cations and Electrolyte pH on the Hydrogen Evolution Reaction on Gold Electrodes in Alkaline Media, Angew. Chem. Int. Ed. 60 (2021) 13452–13462, https://doi.org/10.1002/anie.202102803.
[58] M.C.O. Monteiro, A. Goyal, P. Moerland, M.T.M. Koper, Understanding Cation Trends for Hydrogen Evolution on Platinum and Gold Electrodes in Alkaline Media, ACS Catal. 11 (2021) 14328–14335, https://doi.org/10.1021/acscatal.1c04268.
[59] G.A. El-Nagar, F. Haun, S. Gupta, S. Stojkovikj, M.T. Mayer, Unintended cation crossover influences CO2 reduction selectivity in Cu-based zero-gap electrolysers, Nat. Commun. 14 (2023) 2062, https://doi.org/10.1038/s41467-023-37520-x.
[60] J. Resasco, L.D. Chen, E. Clark, C. Tsai, C. Hahn, T.F. Jaramillo, K. Chan, A.T. Bell, Promoter Effects of Alkali Metal Cations on the Electrochemical Reduction of Carbon Dioxide, J. Am. Chem. Soc. 139 (2017) 11277–11287, https://doi.org/10.1021/jacs.7b06765.
[61] S. Garg, Q. Xu, A.B. Moss, M. Mirolo, W. Deng, I. Chorkendorff, J. Drnec, B. Seger, How alkali cations affect salt precipitation and CO_2 electrolysis performance in membrane electrode assembly electrolyzers, Energ. Environ. Sci. 16 (2023) 1631–1643, https://doi.org/10.1039/D2EE03725D.
[62] J. Wang, Y. Zhao, B.P. Setzler, S. Rojas-Carbonell, C. Ben Yehuda, A. Amel, M. Page, L. Wang, K. Hu, L. Shi, S. Gottesfeld, B. Xu, Y. Yan, Poly(aryl piperidinium) membranes and ionomers for hydroxide exchange membrane fuel cells, Nat. Energy 4 (2019) 392–398, https://doi.org/10.1038/s41560-019-0372-8.